Torsional resonance mode magnetic force microscopy: enabling higher lateral resolution magnetic imaging without topography-related effects

2013 Nanotechnology 24 165704

(http://iopscience.iop.org/0957-4484/24/16/165704)

Nanotechnology **24** (2013) 165704 (7pp) doi:10.1088/0957-4484/24/16/165704

Torsional resonance mode magnetic force microscopy: enabling higher lateral resolution magnetic imaging without topography-related effects

A Kaidatzis and J M García-Martín

IMM—Instituto de Microelectrónica de Madrid (CNM-CSIC), Isaac Newton 8, PTM, E-28760 Tres Cantos, Madrid, Spain

E-mail: andreas.kaidatzis@imm.cnm.csic.es

Received 4 December 2012, in final form 8 March 2013
Published 27 March 2013
Online at stacks.iop.org/Nano/24/165704

Abstract
We present experimental work that reveals the benefits of performing magnetic force microscopy measurements employing the torsional resonance mode of cantilever oscillation. This approach provides two clear advantages: the ability of performing magnetic imaging without topography-related interference and the significant lateral resolution improvement (approximately 15%). We believe that this work demonstrates a significant improvement to a versatile magnetic imaging technique widely used in academia and in industry.

(Some figures may appear in colour only in the online journal)

1. Introduction

The constant need for more and more information storage capacity has driven the miniaturization of magnetic bits in hard disk drives [1], creating the need for a high-resolution magnetic imaging method. Magnetic force microscopy (MFM), a scanning probe technique, has been widely used for this purpose for more than two decades [2, 3]. Currently, the lateral resolution of MFM in ambient conditions is roughly equal to the magnetic bit size of commercial hard disks (≈40 nm). The effort to improve MFM resolution has been focused, up to now, on the fabrication of smaller size MFM probes [4–8]. In this work, we present a different approach to MFM operation that results in improved spatial resolution. It should be noted that, although MFM variations have been implemented (e.g. bimodal MFM [9], switching magnetization MFM [10]), they do not provide any improvement in lateral resolution. Also, other scanning probe magnetic imaging methods that provide high spatial resolution (e.g. spin-polarized scanning tunnelling microscopy [11], ballistic electron emission microscopy [12], magnetic exchange force microscopy [13]) have disadvantages related to the stringent experimental conditions that have to be fulfilled and the restrictions that apply to the possible samples that can be imaged.

Our approach is based on torsional resonance mode atomic force microscopy (TR-AFM), a technique that has emerged during the past decade as a promising dynamic AFM method for imaging lateral forces [14]. Traditional oscillating tip modes of AFM operation, e.g. tapping mode AFM (TM-AFM) [15], employ the flexural (‘diving board’) cantilever vibration. However, TR-AFM takes advantage of the torsional (twisting) cantilever vibration [16]. In a seminal work mainly devoted to analysing tribological and mechanical properties, Kasai *et al* [17] introduced the concept of TR-MFM for imaging in-plane components of the magnetic stray field emanating from the sample, but the potential of this approach has barely been studied. Much more recently, Mühl *et al* [18] also imaged in-plane components of such a stray field, using in this case a sophisticated approach based on the second-order flexural vibrational mode of special probes which require placing a tiny magnet at exactly the nodal point of the cantilever. In our work, we use TR-MFM with home-coated MFM probes that are easily prepared from commercial AFM probes and have a well-defined magnetization which is perpendicular to the sample surface. This approach has allowed us to fully exploit TR-MFM, and it will be shown that it provides two clear advantages over TM-MFM: an ability to obtain magnetic images without interference from surface topography and a significant improvement of magnetic lateral resolution.

2. Experimental details

All measurements were performed in ambient air and room temperature conditions, using a commercial scanning probe microscope (Bruker Dimension Icon operated using the NanoScope 8.10 software). A special, commercially available probe holder was used (Bruker DTRCH), which is composed of two piezoelectric elements that can be excited independently. The elements are excited out-of-phase to perform the TR mode, while in-phase excitation allows execution of the TM mode [19]. The above-mentioned combination of hardware/software provides the ability to perform TR mode measurements. Home-coated MFM probes were used for this study: commercial AFM probes (Nanosensors PPP-FMR, flexural resonance frequency ≈70 kHz, torsional resonance frequency ≈0.7 MHz) were vacuum coated with a 20 nm thick hard magnetic layer ($Co_{80}Cr_{20}$). The layer is deposited at an angle, so that only the back-side of the tip pyramid is coated, thus behaving as a single layer thin film and resulting in a better defined magnetization direction [20]. Tips were magnetized prior to performing measurements using a permanent magnet which applied a magnetic field along the pyramid axis. In fact, in our MFM equipment, as in the majority of commercial MFM equipment, the cantilever is tilted by about 15° with respect to the horizontal. As the opening angle of the back-side of the pyramid is also about 15°, the resulting tip magnetization is perpendicular to the sample surface, as depicted in figure 3(b) of [20]. All microscopy images were processed using the WSxM software [21].

A double-scan MFM method is used (figure 1): first, a TM-AFM scan yields the surface topography. Then, the long-range magnetic forces are detected by a second TR-MFM scan (or a TM-MFM scan, for comparison). In all cases, MFM phase imaging has been performed: the feedback is switched off during the second scan and the phase shift of the cantilever oscillation (resulting from the corresponding resonance frequency shift) is obtained as a signal. Hard disk media were used as samples, as they provide a well-known magnetic structure. A 0.1 Tb m^{-2} longitudinal magnetization hard disk and a 200 Tb m^{-2} perpendicular magnetization hard disk, have been imaged.

3. Results and discussion

3.1. TR-MFM contrast mechanism

Oscillating tip modes of MFM operation employ the detection of cantilever resonance frequency shifts to obtain magnetic contrast. The detected signal in TM-MFM is the shift of the cantilever flexural resonance frequency, which depends on

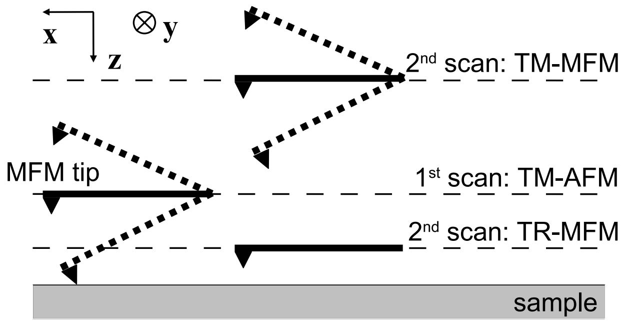

Figure 1. The MFM double-scan method: a first TM-AFM scan yields the surface topography, while the magnetic signal is obtained by a subsequent TM-MFM or TR-MFM scan. The coordinates used throughout this study are also defined.

the z-component magnetic force gradient according to the following equation [22]:

$$\frac{\Delta f}{f_{0,\mathrm{TM}}} = -\frac{1}{2k_{\mathrm{TM}}}\frac{\partial F_z}{\partial z}, \tag{1}$$

where $f_{0,\mathrm{TM}}$ is the initial flexural resonance frequency, Δf is the frequency shift, k_{TM} is the flexural spring constant of the cantilever, and $\partial F_z/\partial z$ is the z-component magnetic force gradient along the z-axis. In this case, the magnetic force that affects the cantilever oscillation occurs due to the interaction between the z-component of the tip magnetization and the z-component of the sample's stray field (or equally, due to the interaction of the z-component of the sample magnetization and the z-component of the tip's stray field). Attractive forces (positive z-component force gradient) result in displacement of the flexural resonance frequency towards lower values, usually coded as dark contrast (the opposite occurs for repulsive forces).

However, the TR mode is sensitive to force gradients along the y-axis and immune to force gradients normal to the sample surface (z-axis) [16]. Moreover, the detected signal in TR-MFM is the shift of the cantilever torsional resonance frequency. It is proposed that this frequency shift depends on the y-component magnetic force gradient, according to the equation:

$$\frac{\Delta f}{f_{0,\mathrm{TR}}} = -\frac{1}{2k_{\mathrm{TR}}}\frac{\partial F_y}{\partial y}, \tag{2}$$

where $f_{0,\mathrm{TR}}$ is the initial torsional resonance frequency, Δf is the frequency shift, k_{TR} is the torsional spring constant of the cantilever, and $\partial F_y/\partial y$ is the y-component magnetic force gradient along the y-axis. In this case, the magnetic force that affects the cantilever oscillation occurs due to the interaction between the y-component of the tip magnetization and the y-component of the sample's stray field.

A comparison between TM-MFM and TR-MFM images, obtained at the same area of the longitudinal magnetization hard disk, is shown in figure 2. The x- and y-axes are indicated in figure 2(a). The cantilever long side and the fast scan axis are along the x-axis. In both cases, the observed contrast is due to the magnetic poles appearing at the domain walls between adjacent magnetic bits (the tip is magnetized along

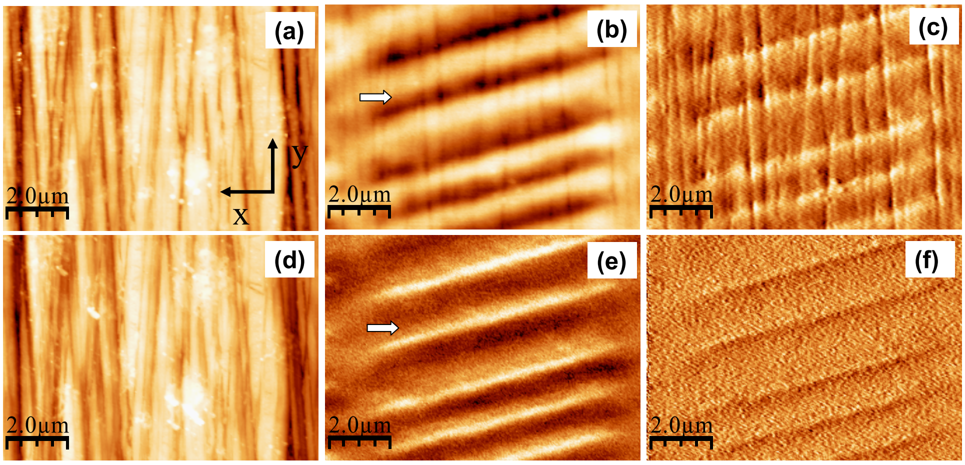

Figure 2. Comparison between TM-MFM and TR-MFM phase imaging of a longitudinal magnetization hard disk. All images were obtained at the same area. (a)–(c) TM-MFM imaging: (a) topography, colour scale: 0.0–68.4 nm. (b) Second scan phase, lift height: 30 nm, colour scale: 0.0°–3.4°. (c) Derivative (x-axis) of second scan phase, colour scale: 0.0–10.6° μm^{-1}. (d)–(f) TR-MFM imaging: (c) topography, colour scale: 0.0–60.0 nm. (d) Second scan phase, lift height: −5 nm, colour scale: 0.0°–0.5°. (f) Derivative (x-axis) of second scan phase, colour scale: 0.0–2.4° μm^{-1}. The white arrows in images (b) and (e) point to the same magnetic structure.

the z-axis and the sample has in-plane magnetization along the y-axis). In both cases, the topography image is obtained simultaneously with the magnetic phase image.

It is interesting to note the contrast reversal between the two modes, something which is not surprising as different components of the magnetic field are probed in each case. In order to facilitate the explanation of the observed signal reversal, a typical case of domain wall contrast in MFM imaging of longitudinal magnetic media is sketched in figure 3. As is explained in [22], the magnetic force gradient along a given direction is equal to the second derivative of the magnetostatic interaction energy. During TM-MFM imaging, the tip is sensitive to the z magnetic field component (see figure 3). In this case, the magnetostatic interaction energy is negative, as it is equal to:

$$E_{\mathrm{TM}} = -\mu_0 \iiint_{\mathrm{tip}} \vec{M}_{\mathrm{tip},z} \cdot \vec{H}_{\mathrm{sam},z} \tag{3}$$

and $\vec{M}_{\mathrm{tip},z}$ is co-directional with $\vec{H}_{\mathrm{sam},z}$ (note that $\vec{M}_{\mathrm{tip},z}$ is equal to $\vec{M}_{\mathrm{tip}}$ since the tip is magnetized along the pyramid axis). Thus, this leads to an attractive interaction.

However, during TR-MFM imaging, the tip is sensitive to the y magnetization component. In this case, although the magnetic field y-axis gradient has a given direction, the y-component of the tip magnetization reverses direction during each cycle due to the torsional tip oscillation, in addition to the lateral tip translation along the y-axis (see figure 3). In a first approximation, the magnetostatic interaction energy, taking into account the two extremities of the oscillation (positions 1 and 2), is given by:

$$E_{\mathrm{TR,total}} = E_{\mathrm{TR},1} + E_{\mathrm{TR},2}, \tag{4}$$

where:

$$E_{\mathrm{TR},1} = -\mu_0 \iiint_{\mathrm{tip}} \vec{M}_{\mathrm{tip},y,1} \cdot \vec{H}_{\mathrm{sam},y,1} \tag{5}$$

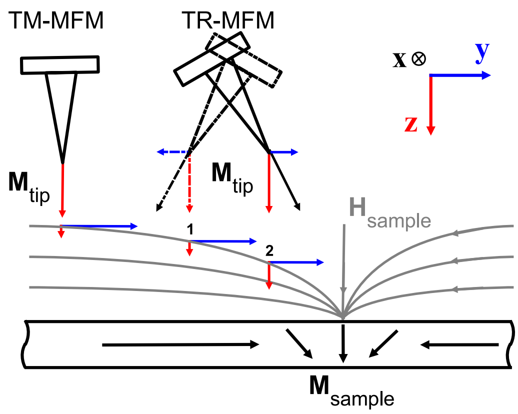

Figure 3. TR-MFM imaging of longitudinal magnetization hard disk.

and:

$$E_{\mathrm{TR},2} = -\mu_0 \iiint_{\mathrm{tip}} \vec{M}_{\mathrm{tip},y,2} \cdot \vec{H}_{\mathrm{sam},y,2}. \tag{6}$$

As $M_{\mathrm{tip},y,1}$ is equal to $M_{\mathrm{tip},y,2}$ and $H_{\mathrm{sam},y,1} > H_{\mathrm{sam},y,2}$, taking into account that $\vec{M}_{\mathrm{tip},y,1}$ and $\vec{M}_{\mathrm{tip},y,2}$ have opposite directions, it can be seen that the total magnetostatic interaction energy in the TR-MFM case is positive, leading to a repulsive interaction (the opposite to that in the TM-MFM case). It is easy to verify that if the domain wall polarity is opposite to that sketched in figure 3, or if the tip magnetization is reversed, the tip–sample interaction would be repulsive for the TM-MFM mode and attractive for the TR-MFM mode. In summary, in any case, there is always contrast reversal between TM-MFM and TR-MFM imaging.

Finally, it should be noted that the TR mode is insensitive to force gradients along the x-axis, thus leading to an absence of TR-MFM contrast when the sample magnetization direction is along the x-axis [17]. This is experimentally shown in figure 4. In the two extreme relative tip–sample

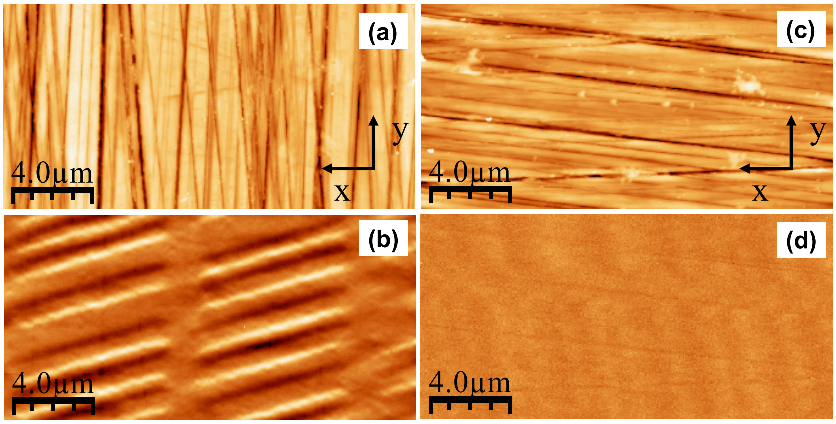

Figure 4. TR-MFM phase imaging of a longitudinal magnetization hard disk. (a), (b) Magnetic bit tracks along the y-axis: (a) topography (b) second scan phase. (c), (d) magnetic bit tracks along the x-axis: (a) topography (b) second scan phase. Colour scale is 0.0–80.0 nm in (a) and (c) and 0.0°–0.7° in (b) and (d). Images obtained at different areas. The lift height is −5 nm in both magnetic images.

orientations, the hard disk tracks are along the y-axis, or along the x-axis. TR-MFM images have been obtained for these two track orientations. The cantilever long side and the fast scan axis are along the x-axis in both cases. In the case of y-axis orientation, the y-axis magnetic force gradient is non-zero, affecting the cantilever oscillation. When the sample is rotated at a 90° angle (tracks and bit magnetization along the x-axis), the y-axis magnetic force gradient is zero and, thus, there is no observed signal. The extremely weak domain wall contrast apparent in figure 4(d) is attributed to non-perfect track alignment along the x-axis.

3.2. *Effect of surface topography*

The double-scan method employed in MFM experiments addresses the issue of distinguishing between the short-range topography-related forces, which are mainly van der Waals forces, and the long-range magnetic forces. While the van der Waals interaction between induced point dipoles falls off as $1/r^6$ (where r is the distance between the two interacting point dipoles), the interaction between magnetic permanent dipoles falls off as $1/r^3$. In practice, van der Waals forces prevail at a distance range up to approximately 10 nm, while they contribute to the measured signal up to a distance of a few tens of nm [22]. In order to tackle this problem, after obtaining the surface topography profile (note that during the first TM-AFM scan the mean tip–sample separation is equal to half of the flexural oscillation amplitude), the tip–sample separation is increased (the tip is 'lifted') up to a point where the van der Waals forces no longer prevail over the magnetic forces (figure 1). This additional tip–sample separation, which is called the 'lift height', is in practice between 20 and 100 nm.

The fact that the main topography-related contrast in MFM images occurs due to the van der Waals forces has an important implication on TR-MFM measurements. Van der Waals forces are central forces, resulting from dipole-type induced interactions [23]. They act along the z-axis, as they are always oriented along a straight line between the two interacting bodies (the tip and the surface in our case). However, as has been shown in the previous section, the TR mode is immune to forces normal to the sample surface (z-axis forces). Thus, TR-MFM is insensitive to the van der Waals interaction and the corresponding topography-related contrast does not contribute to the TR-MFM image.

The above is experimentally demonstrated in figure 2. It is clear that, although topography-related contrast is observed in the TM-MFM image (figure 2(b)), there is no such contribution in the TR-MFM image (figure 2(e)), despite the fact that the tip is 35 nm closer to the sample surface. The tip–surface separation in this case is in the nm-range, where the attractive van der Waals forces dominate every other force field [22, 23]. The negative lift height value at the TR-MFM image indicates that, in this case, the average tip–sample distance during the second scan is actually lower than in the first scan (figure 1). In order to make clear this striking difference between the two magnetic images, figures 2(c) and (f) show the derivatives along the x-axis of the second scan phase signal of the magnetic images. A very intense topography-related contrast appears in the derivative of the TM-MFM image, whereas the only apparent contrast in the derivative of the TR-MFM phase image can be attributed to the magnetic domain walls.

3.3. *Magnetic imaging resolution enhancement*

Besides allowing one to obtain topography-contrast-free magnetic images, TR-MFM also provides resolution enhancement. It is well testified that the lateral resolution of MFM, among other parameters, depends strongly on the tip–surface separation [24]. During TM-MFM measurements two factors determine this distance: the influence of the short range van der Waals forces and the magnitude of the flexural oscillation amplitude. These factors imply that during the second scan the tip should always be farther from the surface than in the first scan.

However, as was shown in the previous paragraphs, van der Waals forces do not affect the torsional cantilever oscillation, eliminating this factor. Moreover, during torsional cantilever excitation, the flexural oscillation is only excited thermally and the corresponding oscillation amplitude is

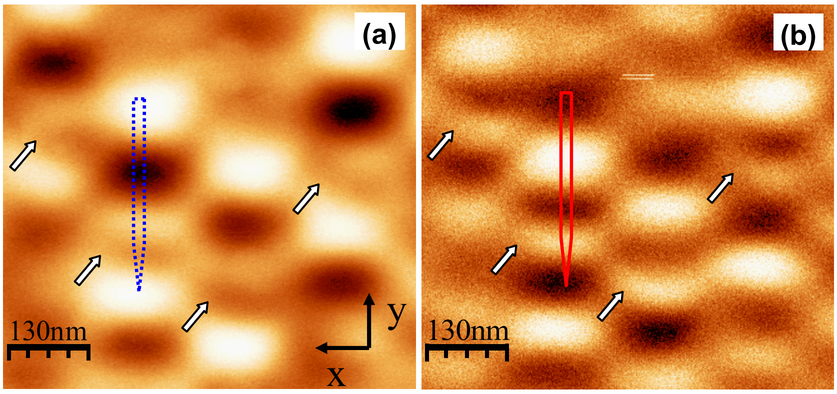

Figure 5. Comparison between TM-MFM and TR-MFM phase imaging of a perpendicular magnetization hard disk. (a) TM-MFM phase image, lift height: 20 nm, colour scale: 0°–2.7°, S/N ratio: 83. (b) TR-MFM phase image, same area as in (a), lift height: −22 nm, colour scale: 0°–0.6°, S/N ratio: 34.

typically around 1 nm (the measured values during this study range between 0.8 and 1.5 nm). From the above, it becomes clear that during the TR-MFM second scan the tip can actually be closer to the sample than in the first scan (figure 1).

This unique advantage of performing TR-MFM measurements at extremely small tip–sample separation is exploited to obtain improved MFM lateral resolution. In order to explore this aspect, the 200 Tb m^{-2} perpendicular magnetization hard disk has been imaged. Perpendicular magnetization arises from a strong out-of-plane magnetic anisotropy, which results in smaller magnetic domains and sharper domain walls, allowing an exploration of the TR-MFM lateral resolution.

In figure 5, TM-MFM and TR-MFM images obtained at exactly the same area of the hard disk, are compared. The TR-MFM image has been obtained immediately after the TM-MFM image, without interrupting scanning. As before, the cantilever long side and the fast scan axis run along the x-axis. The tip is magnetized along the z-axis and the sample out-of-plane magnetization is along the z-axis, thus, the observed contrast is due to the magnetic poles appearing at the domains. The TM-MFM lift height is 20 nm, which is a value at the lower limit of the possible lift heights in TM-MFM measurements. The 'lift' height during TR-MFM is −22 nm (the tip is 22 nm closer to the surface than during the first TM-AFM scan).

Although in the TR-MFM image the signal-to-noise (S/N) ratio is approximately 2.5 times lower than in the TM-MFM image, it is clear that TR-MFM reveals the magnetic structure of the medium in more detail. The magnetic domains have a more rectangular form, while in some cases TR-MFM resolves domains that are barely resolved in the TM-MFM image (e.g. see arrows in figure 5). The absence of topography-related contrast in the TM-MFM is a consequence of the much lower surface roughness of the sample (RMS roughness is 0.4 nm, in contrast to the 11.7 nm in the case of figure 2). The reduced S/N ratio obtained in the TR-MFM image is attributed to the fact that the y-component of the twisting-tip magnetization is much smaller than the z-component (typical torsional angle is less than 1°). It should be noted that, although in each case a different magnetic field

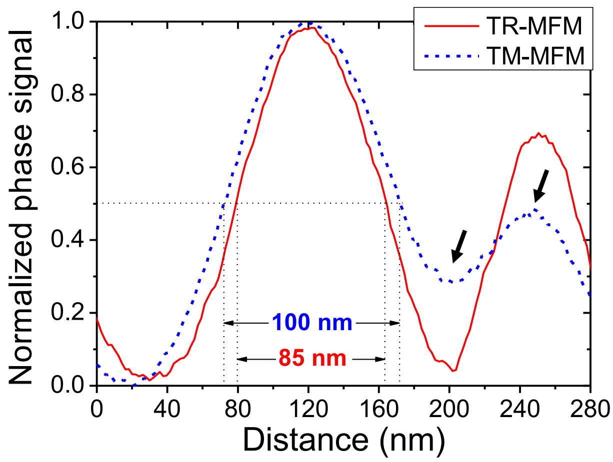

Figure 6. Line profiles obtained in figures 5(a) and (b). Both profiles have been normalized and the TM-MFM profile has been reversed, in order to facilitate comparison. Each curve is an average of 10 profiles, while a 2-point smoothing has been applied to the TR-MFM profile.

component is probed, a direct comparison between the two images can be performed, as the magnetic structure of the medium is unique. In other words, the sources of the stray field are the magnetic poles of the sample; therefore, a MFM image is basically a map of the magnetic poles in the sample [25].

In order to quantify this lateral resolution improvement, line profiles that have been averaged along the directions indicated in figure 5 are shown in figure 6. The peaks and valleys in these profiles correspond to magnetic bits. As can be seen, when comparing the full width at half maximum (FWHM) of the two central bits, the value is decreased from 100 nm in the TM-MFM image, to 85 nm in the TR-MFM image. This corresponds to a lateral resolution improvement of 15%. This improvement can also be deduced from the ability of each technique to resolve between two adjacent bits (see arrows in figure 5). The obtained peak-to-valley contrast is 0.2 in the case of TM-MFM and 0.7 in the case of TR-MFM.

Finally, the effect of the tip–surface separation on the lateral resolution of TR-MFM is discussed. At the beginning

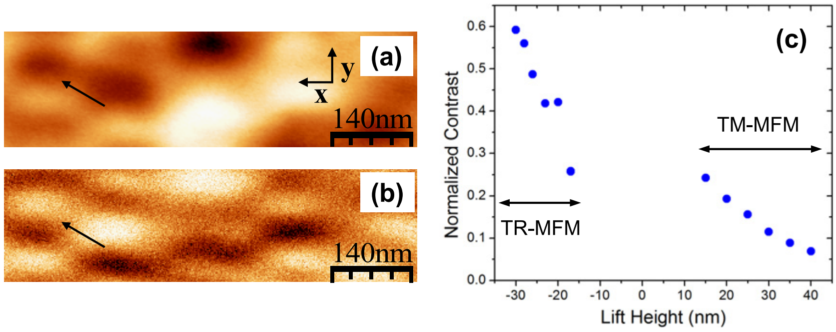

Figure 7. Comparison between TM-MFM and TR-MFM phase imaging of a perpendicular magnetization hard disk. (a) TM-MFM phase image, lift height: 15 nm, colour scale: 0°–3.1°, S/N ratio: 20. (b) TR-MFM phase image, same area as in (a), lift height: −30 nm, colour scale: 0°–0.7°, S/N ratio: 8. (c) Contrast evolution versus lift height, as obtained between the bits indicated in images (a) and (b) by arrows.

of this section it was experimentally shown that TR-MFM exhibits improved lateral resolution compared to TM-MFM, as the tip in the former case is closer to the surface. The evolution of TR-MFM lateral resolution with respect to the tip–surface separation has been studied and the results are discussed in this part (see figure 7).

Series of TM-MFM and TR-MFM images have been obtained at the perpendicular magnetization hard disk, for various tip–sample distances (i.e. the parameter that changed was the lift height). The cantilever long side and the fast scan axis run along the x-axis. The tip is magnetized along the z-axis and the sample out-of-plane magnetization is also along the z-axis, resulting in magnetic bit contrast. All TM-MFM and TR-MFM images have been obtained at exactly the same position of the hard disk. The two best images, which are those obtained with the minimum possible lift height in each case, are shown in figures 7(a) and (b) for TM-MFM (lift height: 15 nm) and TR-MFM (lift height: −30 nm), respectively. The evolution of the magnetic contrast as a function of the lift height is shown for both series in figure 7(c). The peak-to-valley contrast between the two adjacent bits indicated by arrows in figure 7 has been measured for all images and has been normalized to the phase scale in each image (i.e. to the difference between the maximum and the minimum phase signal in the whole image). Once again, one can immediately see the improved resolution of TR-MFM compared to TM-MFM. Moreover, it can be also observed that the TR-MFM resolution increases as the tip approaches the sample surface.

4. Conclusions

In conclusion, the performance of TR-MFM in imaging magnetic structures has been thoroughly studied and it has been shown that it provides two striking advantages over 'conventional' TM-MFM: an ability of obtaining topography-related-free magnetic contrast and, most importantly, a 15% lateral resolution improvement. It is noted that this resolution improvement concerns any magnetic tip, thus, the combination of torsional resonance mode with ultra-sharp magnetic probes can lead to previously unattainable magnetic lateral resolution. Also, the two modes of operation can be performed interchangeably, without needing to interrupt scanning.

Acknowledgments

We gratefully acknowledge stimulating discussions with Mickaël Febvre (Bruker Nano, Inc.). AK received funding from the EC through a FP7 Intra-European Marie Curie post-doctoral Fellowship (Grant No. PIEF-GA-2010-272470). Funding from the Spanish MINECO (refs. MAT2011-29194-C02-01, MAT2010-10213-E and CSD2008-00023) and Comunidad de Madrid (S2009/MAT-1726) is also acknowledged.

References

[1] Wood R 2009 *J. Magn. Magn. Mater.* **321** 555–61
[2] Abraham D W, Williams C C and Wickramasinghe H K 1988 *Appl. Phys. Lett.* **53** 1446–8
[3] Mamin H J, Rugar D, Stern J E, Terris B D and Lambert S E 1988 *Appl. Phys. Lett.* **53** 1563–5
[4] García-Martín J M, Thiaville A, Miltat J, Okuno T, Vila L and Piraux L 2004 *J. Phys. D: Appl. Phys.* **37** 965–72
[5] Koblischka M R, Hartmann U and Sulzbach T 2004 *J. Magn. Magn. Mater.* **272–276** 2138–40
[6] Chen I, Chen L, Gapin A, Jin S, Yuan L and Liou S H 2008 *Nanotechnology* **19** 075501
[7] Amos N, Lavrenov A, Fernandez R, Ikkawi R, Litvinov D and Khizroev S 2009 *J. Appl. Phys.* **105** 07D526
[8] Campanella H, Jaafar M, Llobet J, Esteve J, Vázquez M, Asenjo A, del Real R P and Plaza J A 2011 *Nanotechnology* **22** 505301
[9] Li J W, Cleveland J P and Proksch R 2009 *Appl. Phys. Lett.* **94** 163118
[10] Cambel V, Elias P, Gregusova D, Martaus J, Fedor J, Karapetrov G and Novosad V 2010 *J. Magn. Magn. Mater.* **322** 2715–21
[11] Wiesendanger R, Guntherodt H J, Guntherodt G, Gambino R J and Ruf R 1990 *Phys. Rev. Lett.* **65** 247–50
[12] Kaidatzis A, Rohart S, Thiaville A and Miltat J 2008 *Phys. Rev.* B **78** 174426
[13] Kaiser U, Schwartz A and Weisendnger R 2007 *Nature* **446** 522–5
[14] Su C, Huang L, Prater C B and Bhushan B 2007 Torsional resonance microscopy and its applications *Applied Scanning Probe Methods V* ed B Bhushan, H Fuchs and S Kawata (Berlin: Springer)

[15] Zhong Q, Inniss D, Kjoller K and Elings V B 1993 *Surf. Sci. Lett.* **290** L688–92

[16] Huang L and Su C 2004 *Ultramicroscopy* **100** 277–85

[17] Kasai T, Bhushan B, Huang L and Su C 2004 *Nanotechnology* **15** 731–42

[18] Mühl T, Korner J, Philippi S, Reiche C F, Leonhardt A and Buchner B 2012 *Appl. Phys. Lett.* **101** 112401

[19] Reinstädtler M, Kasai T, Rabe U, Bhushan B and Arnold W 2005 *J. Phys. D: Appl. Phys.* **38** R269–82

[20] Schwarz A and Wiesendanger R 2008 *Nano Today* **3** 28–39

[21] Horcas I, Fernández R, Gómez-Rodríguez J M, Colchero J, Gómez-Herrero J and Baro A M 2007 *Rev. Sci. Instrum.* **78** 013705

[22] Thiaville A, Miltat J and García-Martín J M 2005 Magnetic force microscopy: images of nanostructures and contrast modelling *Magnetic Microscopy of Nanostructures* ed H Hopster and H P Oepen (Berlin: Springer)

[23] Goodman F O and Garcia N 1991 *Phys. Rev.* B **43** 4728–31

[24] Wadas A and Grutter P 1989 *Phys. Rev.* B **39** 12013–7

[25] Hubert A, Rave W and Tomlinson S L 1997 *Phys. Status Solidi* b **204** 817–28